

# HNPS Advances in Nuclear Physics

Vol 30 (2024)

HNPS2023



## Covariant density functional description of shape phase transitions and shape coexistence in heavy nuclei

Vaia Prassa, Konstantinos Karakatsanis

doi: [10.12681/hnpsanp.6284](https://doi.org/10.12681/hnpsanp.6284)

Copyright © 2024, Vaia Prassa, Konstantinos Karakatsanis



This work is licensed under a [Creative Commons Attribution-NonCommercial-NoDerivatives 4.0](https://creativecommons.org/licenses/by-nc-nd/4.0/).

### To cite this article:

Prassa, V., & Karakatsanis, K. (2024). Covariant density functional description of shape phase transitions and shape coexistence in heavy nuclei. *HNPS Advances in Nuclear Physics*, 30, 75–80. <https://doi.org/10.12681/hnpsanp.6284>

# Covariant density functional description of shape phase transitions and shape coexistence in heavy nuclei

V. Prassa\*, K.E. Karakatsanis

*Physics Department, Faculty of Science, University of Thessaly, 3<sup>rd</sup> Km Old National Road, 35100, Lamia, Greece*

---

**Abstract** The phenomena of shape phase transitions and shape coexistence in even-even heavy nuclei are analysed within the covariant density functional framework. Spectroscopic observables that characterize low-lying collective excitations associated with order parameters are computed using the corresponding generalized microscopic collective Hamiltonians with deformations as dynamical collective coordinates. The parameters of the Hamiltonians are determined by relativistic Hartree-Bogoliubov calculations based on the energy density functional DD-PC1, and a finite-range pairing interaction.

**Keywords** Covariant density functional theory, shape coexistence, shape phase transitions, collective Hamiltonian.

---

## INTRODUCTION

The study of shape phase transitions and shape coexistence represents a highly active area of research in low-energy nuclear physics, as highlighted in Refs. [1–7]. These phenomena can manifest in light, medium-heavy, heavy, and superheavy nuclei, providing valuable insights into the organization of nucleons in finite nuclei. In their ground state configuration, the majority of nuclei deviate from spherical shapes, often displaying quadrupole deformed shapes resulting from strong proton-neutron correlations in open-shell nuclei with axial and reflection symmetry. Additionally, less frequently, nuclei exhibit “pear-like” octupole shapes, either in a stable or dynamic manner, arising from the spontaneous breaking of their intrinsic reflection symmetry.

In certain regions of the nuclear chart, the evolution of equilibrium shapes with variations in nucleon number can undergo sudden changes, leading to phenomena such as shape coexistence and quantum phase transitions. The density functional theory [8,9] serves as a unified and comprehensive framework for describing nuclear shapes across the entire nuclear chart. Within this framework, the manuscript presents recent findings [10] derived from studies on nuclear shape phase transitions and shape coexistence using covariant density functional theory (CDFT) [9].

## STRUCTURAL EVOLUTION IN THE NEUTRON DEFICIENT MERCURY ISOTOPES

In the vicinity of  $Z=82$ , particularly near the neutron midshell  $N=104$ , the phenomena of shape coexistence and phase transitions were initially identified in studies of hyperfine structure [11]. Later spectroscopic investigations [12–23] revealed that the structure of isotopes in this region is characterized by intruder prolate deformed configurations coexisting with less deformed oblate ground states. The low-lying excited states of the intruder band exhibit a parabola shape as a function of neutron number, starting from  $^{188}\text{Hg}$  down to the midshell at  $N=104$ , with a minimum observed at  $^{182}\text{Hg}$  and going up to  $^{180}\text{Hg}$  and  $^{178}\text{Hg}$  [24,25]. In contrast, in the heavier transitional isotopes with  $190 < A < 200$ , the energy levels of the yrast band exhibit minimal variation.

This contribution presents constrained self-consistent mean field (SCMF) calculations for even-even isotopes of  $^{176-190}\text{Hg}$  within the relativistic Hartree-Bogoliubov [9] method. The calculations employ the density-dependent point-coupling (DD-PC1) [26] energy density functional in the particle-

---

\* Corresponding author: [vprassa@uth.gr](mailto:vprassa@uth.gr)

hole channel and a separable pairing force [27] in the particle-particle channel. In this analysis, the pairing strength was adjusted individually for each Hg isotope to reproduce the odd-even staggering effect, resulting in an increase by a factor of 10-20%, depending on the specific isotope.

To illustrate the rapid change of equilibrium shapes, Fig. 1 presents the potential energy surfaces (PES) of even-even isotopes  $^{176-190}\text{Hg}$ . Starting with the lighter isotopes,  $^{176}\text{Hg}$  and  $^{178}\text{Hg}$ , the energy surfaces exhibit  $\gamma$ -soft characteristics with small oblate deformations. In  $^{180}\text{Hg}$  a second prolate deformed minimum emerges on the potential surface, becoming the dominant one in  $^{182}\text{Hg}$ . The energy surfaces of  $^{184}\text{Hg}$  and  $^{186}\text{Hg}$  display a relatively flat profile in the  $\gamma$ -direction, with two minima at an energy difference of 500 keV, indicating a case of shape coexistence between the two different configurations. The equilibrium configuration is prolate in  $^{184}\text{Hg}$  and oblate in  $^{186}\text{Hg}$ . The prolate minimum diminishes in  $^{188-190}\text{Hg}$ , and the isotopes become oblate deformed. For all isotopes, the ground state configurations are oblate deformed, except for  $^{182}\text{Hg}$  and  $^{184}\text{Hg}$  which exhibit a prolate deformation.

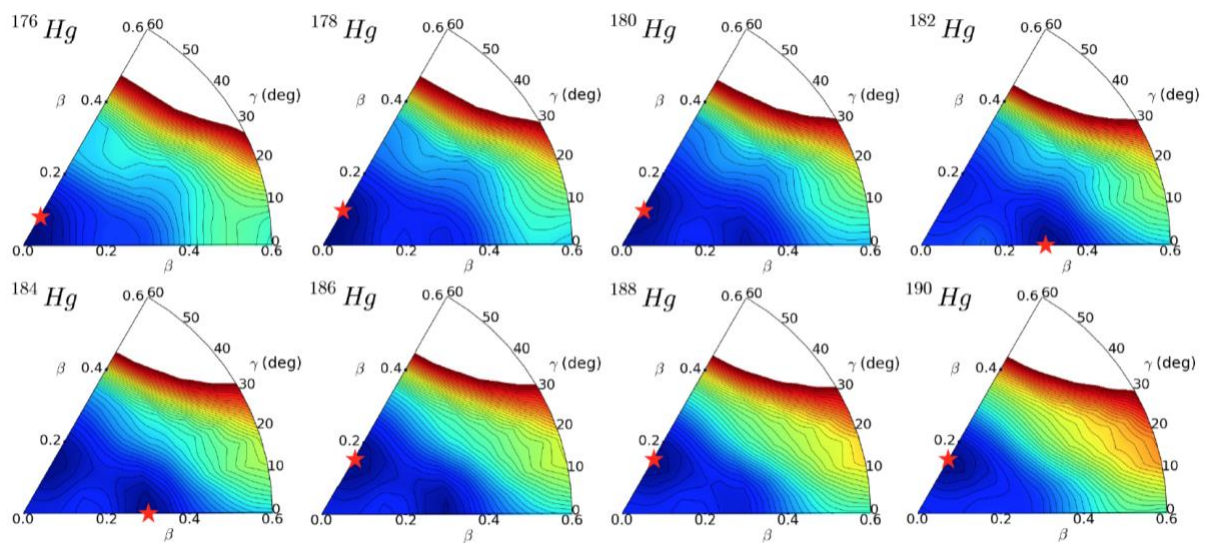


**Figure 1.** Self-consistent RHB triaxial quadrupole energy surfaces of even-even  $^{176-190}\text{Hg}$  isotopes in the  $\beta$ - $\gamma$  plane ( $0^\circ < \gamma < 60^\circ$ ). All energies are normalized with respect to the binding energy of the corresponding ground state.

A five-dimensional collective Hamiltonian (5DCH) with quadrupole deformations as dynamical collective coordinates [28,29] is used to calculate the low-energy excitation spectrum. The microscopic self-consistent solutions of deformation-constrained triaxial relativistic Hartree-Bogolyubov (RHB) calculations, the single particle wave functions, occupation probabilities, and quasiparticle energies, are used to calculate the Hamiltonian parameters. The moments of inertia are calculated with the Inglis-Belyaev formula [30,31] and the mass parameters with the cranking approximation [32]. The collective potential is obtained by subtracting the zero-point energy corrections [32] from the total energy that corresponds to the solution of constrained triaxial SCMF calculations. The resulting collective potential and inertia parameters as functions of the collective coordinates determine the dynamics of the 5DCH.

In Fig. 2, the excitation energy systematics for isotopes  $^{176-200}\text{Hg}$ , obtained with the 5DCH, are presented. The model successfully reproduces the nearly parabolic trend observed in the energy levels of  $^{176}\text{Hg}$  up to  $^{190}\text{Hg}$ , a crucial feature experimentally interpreted as indicative of shape coexistence in these isotopes (see Fig. 10 of Ref. [6]). Conversely, a relatively flat behavior in the excitation energies is observed with increasing neutron number for the heavier Hg nuclei ( $A > 190$ ), aligning well with experimental data. A noteworthy observation is the near-degeneracy between the levels of the excited band and the levels of the ground state with two additional units of angular momentum. Specifically,

pairs of levels such as  $4^+_{1/2+2}$ ,  $6^+_{1/4+2}$ ,  $8^+_{1/6+2}$ , and so on, exhibit almost the same energy in  $^{176-186}\text{Hg}$ , signaling configuration mixing. This phenomenon is more pronounced in the spectrum of neutron-deficient Pb isotopes around  $N=104$  (see Fig. 12 of Ref. [6]). Additionally, the model captures the lowest excitation energy of the second  $0^+_2$  state at  $N=102$  ( $A=182$ ), close to the neutron midshell. A structural change is observed in the energy spectrum from  $^{192}\text{Hg}$  to  $^{194}\text{Hg}$ , corresponding to the disappearance of the prolate minimum and increased stiffness of the potential around the oblate equilibrium point. Furthermore, the calculated spectra for  $^{176}\text{Hg}$  and  $^{178}\text{Hg}$  display a vibrational-like behavior with  $R_{4/2} = E(4^+_{1/2})/E(2^+_{1/2})$  ratios around 1.9, and close-lying  $4^+_{1/2}$ ,  $2^+_{2/2}$ , and  $0^+_{2/2}$  levels, indicative of a vibrational level structure. On the other hand, isotopes with  $180 < A < 192$  are  $\gamma$ -soft, consistent with the respective potential energy surfaces at the mean-field level.

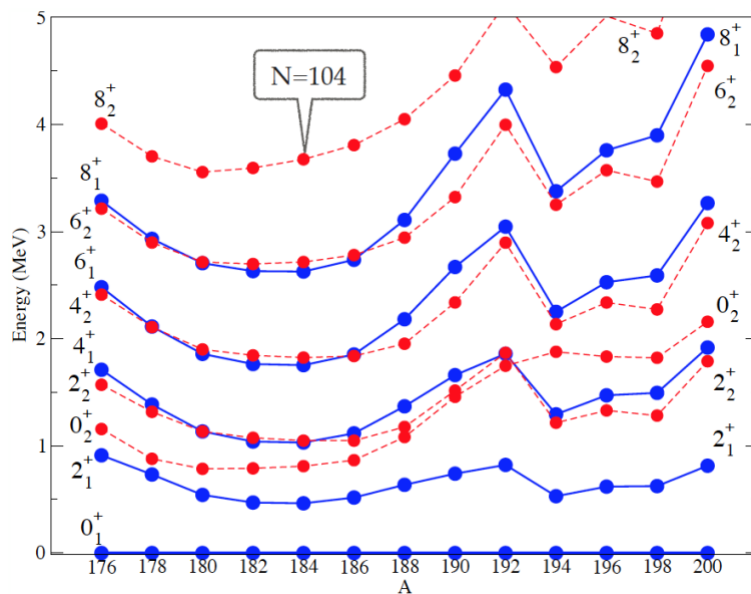


**Figure 2.** Energy systematics of the low-lying excited states in even-even neutron-deficient mercury isotopes. The blue lines correspond to the levels of the ground state band, while the red ones to the excited band.

## OCTUPOLE SHAPE PHASE TRANSITIONS IN NEUTRON RICH ACTINIDES

In the case of actinides with atomic number  $Z \sim 96$  and neutron number  $N \sim 196$ , the coupling of neutron orbitals  $h_{11/2}$  and  $k_{17/2}$ , along with the coupling of proton single-particle states  $f_{7/2}$  and  $i_{13/2}$ , can give rise to octupole deformations. This study focuses on the analysis of shape phase transitions and critical points in octupole-deformed neutron-rich actinides, specifically Cm, Cf, Fm, and No. A microscopic realization of a quantum phase transition (QPT) from non-octupole to stable octupole deformation and to octupole vibrations is presented.

The analysis employs the axially reflection-asymmetric implementation of the relativistic Hartree-Bogoliubov (RHB) model [33-35] and the quadrupole-octupole collective Hamiltonian (QOCH) [33-35]. These models are constructed to calculate excitation spectra and observables associated with quantum order parameters. The mean-field potential in this analysis is determined by the relativistic density functional DD-PC1 [26] in the particle-hole channel, while a separable pairing force [27] is utilized in the particle-particle channel. The calculations presented here have been partially discussed in [10].

Already at the mean-field level the RHB model predicts a very interesting structural evolution with transitions from non-octupole to pronounced octupole deformations and to shallow  $\beta_3$  potentials, as illustrated in Fig. 3. In the case of  $^{282}\text{Cm}$  the potential energy surface is softer, with the energy minimum at  $(\beta_2, \beta_3) \sim (0, 0)$ . With the increase of neutron number more pronounced quadrupole and octupole



deformations develop. For  $^{288}\text{Cm}$  with  $N=192$  the energy minimum is found in the non-zero octupole deformation region, located at  $(\beta_2, \beta_3) \sim (0.09, 0.14)$ . The potentials become more rigid in  $\beta_2$  and softer in  $\beta_3$ . The maximum gain in binding energy due to octupole deformation is found in  $^{292}\text{Cm}$  at neutron number  $N=196$ .

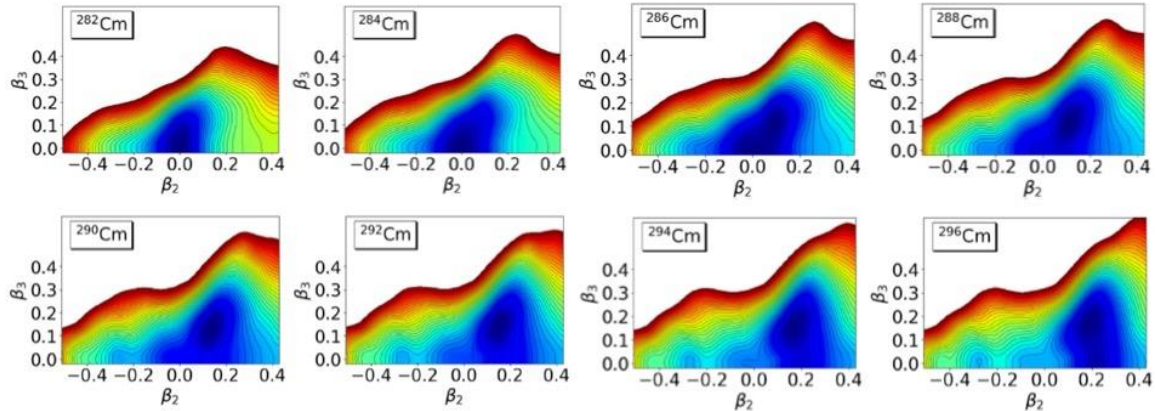


**Figure 3.** Microscopic DD-PC1 self-consistent relativistic Hartree-Bogoliubov axially symmetric energy surfaces of the nuclei  $^{282-296}\text{Cm}$  in the  $(\beta_2, \beta_3)$ -plane. The contours join points on the surface with the same energy and the separation between neighboring contours is 0.5 MeV.

To quantitatively investigate shape transitions and critical point phenomena, it is essential to move beyond a simple Kohn-Sham approximation and consider the restoration of broken symmetries at the mean-field level, along with fluctuations in collective coordinates. Spectroscopic properties relevant for characterizing shape transitions are examined using a quadrupole-octupole collective Hamiltonian, which is a gamma-rigid axially symmetric version of the general quadrupole-octupole Bohr Hamiltonian.

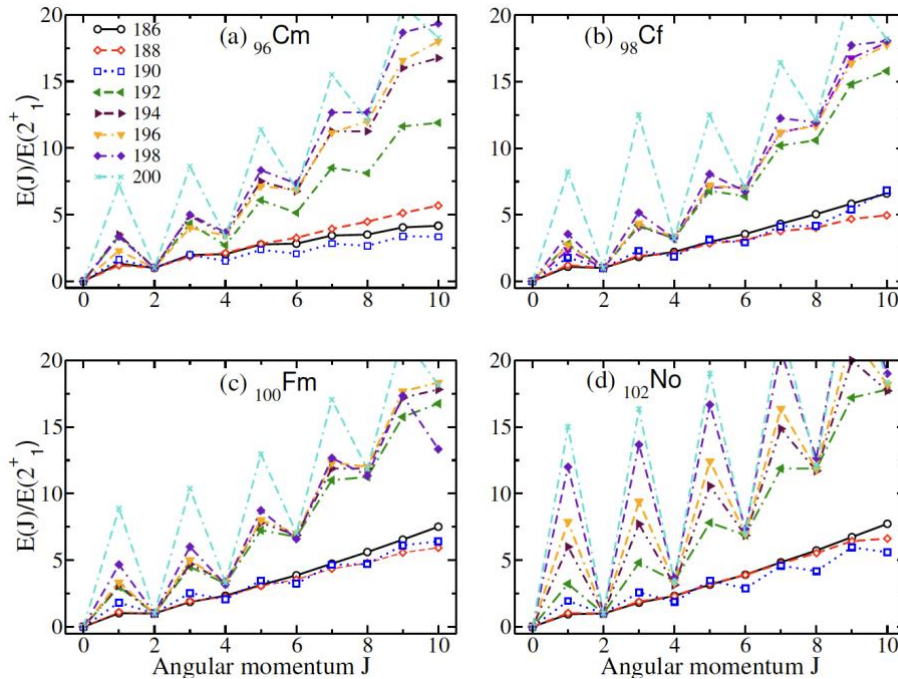


**Figure 4.** (Color online) Theoretical energy ratios  $E(J^\pi)/E(2^+_1)$  of the yrast states of (a)  $^{96}\text{Cm}$ , (b)  $^{98}\text{Cf}$ , (c)  $^{100}\text{Fm}$ , and (d)  $^{102}\text{No}$ , including both positive ( $J$  even) and negative ( $J$  odd) parity, as functions of  $J$ .

The odd-even staggering in the energy ratio  $E(J^\pi)/E(2^+_{11})$ , where  $\pi=+$  for even-spin and  $\pi=-$  for odd-spin yrast states, serves as evidence of phase transitions from non-octupole to octupole deformation and octupole vibrations, particularly for shallow  $\beta_3$  potentials. If an alternating-parity rotational band is formed, the energy ratio would depend quadratically on  $J$ . However, if the even-spin and odd-spin yrast states constitute a separate rotational band built on the octupole vibration, the ratio is expected to exhibit a pronounced odd-even-spin staggering. In Fig. 4, the ratios  $E(J^\pi)/E(2^+_{11})$  for both positive- and negative-parity yrast states of  $^{282-296}\text{Cm}$ ,  $^{284-298}\text{Cf}$ ,  $^{286-300}\text{Fm}$  and  $^{288-302}\text{No}$  are displayed as functions of the angular momentum  $J$ . Notably, the odd-even staggering is negligible for  $N<190$  in all isotopic chains, with the  $\pi=+$  and  $\pi=-$  states lying close in energy, indicating they merge into a single band. The staggering becomes more pronounced starting at  $N=192$ , suggesting the onset of octupole vibrations, where the negative-parity band is a separate rotational band built on the octupole bandhead. For isotopes with  $N=186-190$  close to the neutron shell closure at  $N=184$ , the equidistant energy levels signify a quadrupole vibrational structure with  $E(4^+_{11})/E(2^+_{11}) \sim 2$ . On the other hand, for heavier nuclei with  $N>194$ , the behavior is of rotational type  $L(L+1)$  with  $E(4^+_{11})/E(2^+_{11}) \sim 3.33$ . Specifically, for  $^{288}\text{Cm}_{192}$ , the  $E(4^+_{11})/E(2^+_{11})$  ratio is approximately 2.7, close to the value 2.71 predicted by the X(4) model [36], suggesting a critical point of a quadrupole phase transition between spherical and quadrupole-deformed prolate shapes. Any discrepancy could be attributed to missing triaxial correlations in the QOCH. These results signify shape phase transitions from non-octupole to stable octupole deformations and to octupole vibrations as a function of the control parameter –the neutron number. The energy ratio  $E(J^\pi)/E(2^+_{11})$  can be considered as an order parameter for the octupole shape transition.

## CONCLUSIONS

The covariant density functional framework has been applied to study the phenomena of shape phase transitions and shape coexistence in neutron rich actinides and neutron deficient mercury isotopes.

In the case of neutron deficient even-even Hg isotopes the self-consistent mean field calculations suggest configuration mixing and shape coexistence already at the mean field level. This can be further supported by extending the analysis beyond the mean field, employing a quadrupole collective Hamiltonian. The systematics of the low-lying energy levels of the excited states exhibit a parabolic trend for isotopes with  $178<A<190$ , reaching a minimum at  $^{182}\text{Hg}$  ( $N=102$ ). Additionally, the levels of the excited band are nearly degenerate with the levels of the ground state but with two units of angular momentum higher. Specifically, pairs such as  $4^+_{11}/2^+_{12}$ ,  $6^+_{11}/4^+_{12}$ ,  $8^+_{11}/6^+_{12}$  have identical energy values. These features are characteristic and align with experimental observations in isotopes of Hg and Pb, where shape coexistence is a well-established phenomenon.

In the neutron-rich actinides, specifically Cm, Cf, Fm, and No with neutron numbers  $186<N<200$ , results obtained using the relativistic Hartree-Bogoliubov model and a collective quadrupole-octupole Hamiltonian indicate phase transitions from non-octupole to octupole deformed shapes and to octupole vibrations. Critical points for these transitions are identified at neutron numbers  $N=192$  and  $N=196$ , respectively. Within the isotopic chain of Cm, the calculations suggest the onset of a double phase transition from spherical to quadrupole-deformed and from non-octupole to octupole-deformed shapes. Notably,  $^{288}\text{Cm}$  is identified as being closest to the critical point. The neutron-rich actinides under consideration exhibit a complex structure with octupole and triaxially deformed shapes. A more comprehensive description of their properties would necessitate model extensions capable of handling the reflection asymmetric degree of freedom and triaxial deformation simultaneously. Experimental studies in this region would be crucial in identifying any deficiencies in the model, such as missing degrees of freedom or shortcomings in describing underlying shell structures and pairing correlations.

## References

- [1] K. Heyde, P. Van Isacker, M. Waroquier, J.L. Wood, and R.A. Meyer, *Phys. Rep.* 102, 291 (1983)
- [2] J.L. Wood, K. Heyde, W. Nazarewicz, M. Huyse, and P. Van Duppen, *Phys. Rep.* 215, 101 (1992)
- [3] A.N. Andreyev, M. Huyse, P. Van Duppen, et al., *Nature (London)* 405, 430 (2000)
- [4] R. Julin, K. Helariutta, and M. Muikku, *J. Phys. G* 27, R109 (2001)
- [5] T. Grahm, A et al., *Nucl. Phys. A* 801, 83 (2008)
- [6] K. Heyde and J.L. Wood, *Rev. Mod. Phys.* 83, 1467 (2011)
- [7] P. Cejnar, J. Jolie, and R. F. Casten, *Rev. Mod. Phys.* 82, 2155 (2010)
- [8] M. Bender, Heenen P-H and Reinhard P-G 2003 *Rev. Mod. Phys.* 75 121
- [9] D. Vretenar, A.V. Afanasjev, G.A. Lalazissis and P. Ring, *Phys. Rep.* 409 101 (2005)
- [10] V. Prassa, *EPJ A* 58, 183 (2022)
- [11] J. Bonn et al, *Phys. Lett. B* 38, 308 (1972)
- [12] N. Rud et al, *Phys. Rev. Lett.* 31, 1421 (1973)
- [13] D.Proetel, R. M. Diamond, and F.S. Stephens, *Phys. Lett. B* 48, 102 (1974)
- [14] Hamilton, J. H., et al., *Phys. Rev. Lett.* 35, 562 (1975)
- [15] Cole, J. D., et al., *Phys. Rev. Lett.* 37, 1185 (1976)
- [16] G.D. Dracoulis, *Phys. Scr.* 2000, 54 (2000)
- [17] N. Bree, et al, *Phys. Rev. Lett.* 112, 162701 (2014)
- [18] L.P. Gaffney, M. Hackstein, R.D. Page, et al., *Phys. Rev. C* 89, 024307 (2014)
- [19] R. Julin et al, *J. Phys. G* 43, 024004 (2016)
- [20] B. A. Marsh, T. Day Goodacre et al., *Nat. Phys.* 14, 1163 (2018)
- [21] A. Esmaylzadeh et. al., *Phys. Rev. C* 98, 044306 (2018)
- [22] S. Sels, T. Day Goodacre, B.A. Marsh et al., *Phys.Rev. C* 99, 044306 (2019)
- [23] B. Olaizola et. al., *Phys. Rev. C* 100, 024301 (2019)
- [24] C. Müller-Gatermann et al., *Phys. Rev. C* 99, 054325 (2019)
- [25] J. Elseviers, A.N. Andreyev, et al., *Phys. Rev. C* 84, 034307 (2011)
- [26] T. Nikšić, D. Vretenar, and P. Ring, *Phys. Rev. C* 78, 034318 (2008)
- [27] Y. Tian, Z.Y. Ma, and P. Ring, *Phys. Lett. B* 676, 44 (2009)
- [28] Z.P. Li, T. Nikšić, D. Vretenar, P. Ring, and J. Meng, *Phys. Rev. C* 81, 064321 (2010)
- [29] T. Nikšić, D. Vretenar, and P. Ring, *Prog. Part. Nucl. Phys.* 66, 519 (2011)
- [30] D. Inglis, *Phys. Rev.* 103, 1786 (1956)
- [31] S. Beliaev, *Nucl. Phys.* 24, 322 (1961)
- [32] M. Girod and B. Grammaticos, *Nucl. Phys. A* 330, 40 (1979)
- [33] Z.P. Li, B.Y. Song, J.M. Yao, D. Vretenar, J. Meng, *Physics Letters B* 726 866869 (2013)
- [34] S.Y. Xia, H. Tao, Y. Lu, Z.P. Li, Niksic, and D. Vretenar, *Phys. Rev. C* 96, 054303 (2017)
- [35] Z. Xu and Z.-P. Li, *Chin. Phys. C* 41, 124107 (2017)
- [36] R. Budaca, A.I. Budaca, *Phys. Lett. B* 759, 349 (2016)